The Astrophysical Journal, 922:133 (7pp), 2021 December 1 https://doi.org/10.3847/1538-4357/ac3239

Radiative Association between Neutral Radicals in the Interstellar Medium: $CH_3 + CH_3O$

Jessica Tennis[1], Jean-Christophe Loison[2], and Eric Herbst[1,3]
[1] Department of Chemistry, University of Virginia, Charlottesville, VA 22904 USA; jdt6mp@virginia.edu
[2] Université de Bordeaux, ISM, CNRS UMR 5255, F-33400 Talence, France
[3] Department of Astronomy, University of Virginia, Charlottesville, VA 22904 USA
Received 2021 August 3; revised 2021 October 19; accepted 2021 October 20; published 2021 November 26

Abstract

Uncertainties in the production mechanisms of interstellar complex organic molecules call for a precise investigation of gas-phase synthetic routes for these molecules, especially at low temperatures. Here, we report a study of the gas-phase formation of dimethyl ether from the neutral radicals methyl and methoxy via the process of radiative association. This process may be important to synthesize dimethyl ether and species such as methyl formate, for which dimethyl ether is a precursor. The reaction is found to be rapid by the standards of radiative association, especially at 10 K, where its rate coefficient is calculated by two different methods to be 3×10^{-11} or 2×10^{-10} cm^3 s^{-1}; the lower rate is calculated with a more precise theory and is likely more accurate. Insertion of this reaction into the Nautilus network is found not to explain fully the abundance of dimethyl ether in cold and prestellar cores, especially in those cores with the highest dimethyl ether abundances.

Unified Astronomy Thesaurus concepts: Astrochemistry (75); Reaction rates (2081); Interstellar molecules (849)

1. Introduction

The interstellar medium (ISM) owes much of its chemical complexity to grain-surface processes. As the known diversity of larger gas-phase species in the ISM continues to increase, however, new production mechanisms for complex organic molecules (COMs) must be investigated. Garrod et al. (2008) have shown that complex organic molecules can be formed efficiently on the surfaces of cold grains at temperatures as low as 20–30 K in star-forming regions, and that as these systems continue to develop and warm up, thermal desorption increases the gas-phase abundance of COMs. Thus, molecules formed on the grain become detectable in the gas phase. Recently, COMs have been observed in cold and prestellar cores at temperatures as low as 10 K despite the difficulty of diffusive formation on grains at this temperature as well as the need for nonthermal desorption mechanisms to detect the species (Cernicharo et al. 2010; Öberg et al. 2010; Bacmann et al. 2012; Jaber et al. 2014; Vastel et al. 2014). Balucani et al. (2015) and Vasyunin & Herbst (2013) have shown that neutral–neutral gas-phase reactions can play an important role in the formation of COMs. The radiative association of neutral radical species is a particularly good candidate for increasing chemical complexity because of the inverse temperature dependence of its rate coefficient and the high relative abundance of neutral species compared with ions in the interstellar medium (ISM).

Radiative association occurs via the stabilization of a collision complex, or unstable intermediate species, by the emission of a photon. The collision complex, a species that sits above a local potential minimum, is formed by the exothermic association of two gas-phase species, and the process benefits from the inverse temperature dependence of its rate coefficient and the much smaller timescales of radiative stabilization as compared with collisional stabilization in the low densities of cold, dark clouds. Competitive dissociation and reaction mechanisms must still be considered in the calculation of a radiative association rate coefficient.

One of the COMs detected in several cold and prestellar cores is dimethyl ether (CH_3OCH_3). It has been seen at a relative abundance of 2×10^{-11} toward the cold, dense core B1-b (Cernicharo et al. 2010), 2.5×10^{-10} toward the cyanopolyyne peak in TMC-1 (Agúndez et al. 2021) and 1.5×10^{-10} at its main peak (Soma et al. 2018), 1.3×10^{-10} around the dense core L483 (Agúndez et al. 2019), 2×10^{-11} in the prestellar core L1689B (Bacmann et al. 2012), and 7×10^{-10} toward the Barnard 5 molecular cloud (Taquet et al. 2017). Although a number of different formation routes have been reported in the literature, it is unclear that the abundance of dimethyl ether is fully understood. One possibility reported but not treated in detail is radiative association.

The radiative association to form dimethyl ether is thought to occur via the association of the radicals methyl (CH_3) and methoxy (CH_3O) (Vasyunin & Herbst 2013; Balucani et al. 2015). Both dimethyl ether and the methoxy radical have been observed in cold, dark clouds while the nonpolar methyl radical has been detected toward the galactic center in the infrared, but not in a cold dark cloud (Feuchtgruber et al. 2000; Cernicharo et al. 2010; Öberg et al. 2010; Bacmann et al. 2012; Jaber et al. 2014). The dimethyl ether collision complex formed by association of the neutral methyl and methoxy radicals has several output channels all located above the input channel except for the roaming, as previously calculated by Sivaramakrishnan et al. (2011). This roaming pathway describes the bimolecular pathway leading from $CH_3 + CH_3O$ to $CH_4 + H_2CO$ well with a high rate at room temperature (around 2×10^{-11} cm^3 s^{-1}; Tsang & Hampson 1986; Sivaramakrishnan et al. 2011) even if there is also a direct pathway leading to $CH_4 + H_2CO$. This direct pathway does not involve the formation of CH_3OCH_3 and is not considered in this work. Note that in addition to the paths computed by Sivaramakrishnan et al. (2011), there is a very high barrier on the competitive exit path toward dissociation into methane and formaldehyde (around

1.4 eV above the $CH_3 + CH_3O$ energy), making association much more likely than the bimolecular exit path and making this system particularly interesting to study.

Previous estimates of the reaction rate coefficient between the methyl and methoxy radicals vary but indicate that the rate coefficient of this reaction could be sufficiently large to explain the abundance of dimethyl ether and its daughter product methyl formate (Vasyunin & Herbst 2013; Balucani et al. 2015). Here, the previous approaches are compared with a microcanonical as well as a less detailed canonical calculation. The microcanonical approach is likely to be more accurate for interstellar environments, which often cannot be represented well by one average temperature (Herbst 1985). Our microcanonical approach uses the phase-space model, which conserves angular momentum and energy in the calculation of association and dissociation probabilities.

2. Theory

As noted earlier, the concentration of the collision complex is governed by a number of processes, which include formation, redissociation back into reactants, production of bimolecular products, and stabilization by radiative emission and, at higher densities, collisional stabilization. Each of these several steps has an associated rate coefficient. Under the steady state assumption, the overall microcanonical rate coefficient k_{ra} for radiative association is given by the equation (Herbst 1985):

$$k_{ra}(J_A, J_B, J, E) = \frac{k_1(J_A, J_B, J, E)k_r}{k_{-1}(J, E) + k_r + k_2(J, E)}, \quad (1)$$

where J is the total angular momentum, k_1 is the association rate coefficient for the reactants to form a complex, k_r is the radiative stabilization rate, k_{-1} is the rate at which the complex redissociates into the precursors, and k_2 is the rate at which the complex dissociates into new products. The rate coefficient for complex formation is given by the equation

$$k_1 = v\sigma, \quad (2)$$

where σ is the phase-space cross section (Light 1967; Herbst 1987) and v is the relative velocity between the two reactants. This cross section sums over all possibilities up to a maximum value of the collisional angular momentum L, for fixed values of the angular momenta J_A and J_B of the reactants A and B, as shown in the equation

$$\sigma = \left(\frac{\pi h^2 G}{2\mu E_{coll}}\right)\sum_{L=0}^{L_{max}}(2L + 1)P(J). \quad (3)$$

Here G is the ratio of the electronic degeneracy of the complex to that of the reactants assuming the reactants are in the ground electronic state, μ is the reduced mass of the reactants, E_{coll} is the collisional energy of the reactants, and $P(J)$ is the probability that the complex is formed with a particular total angular momentum J, as given by

$$P(J) = \sum_{J_r}\frac{(2J + 1)}{(2J_r + 1)(2L + 1)}\frac{(2J_r + 1)}{(2J_A + 1)(2J_B + 1)}, \quad (4)$$

where J_r is the result of the vector sum of J_A and J_B, which then combines vectorially with L to form the total angular momentum J. L_{max} is the collisional angular momentum at which the peak of the centrifugal barrier of the attractive potential equals the translational energy of the reactants, so that an excess of angular momentum does not tear the collision complex apart (Light 1967).

The choice of a potential for our calculation is difficult to decide. Long-range isotropic capture potentials are simple but may be less accurate than anisotropic potentials especially with short-range effects. Anisotropic neutral–neutral potentials at long and short range as well as attractive and repulsive terms for such systems were tested by Liao & Herbst (1995) for the reactions $CN + C_2H_2$ and $C + C_2H_2$. These systems had been studied in the laboratory, the CN system from room temperature down to low temperatures near 25 K, and the C reaction at room temperature. Liao & Herbst (1995) found that the effect of long-range anisotropy and short-range repulsion on isothermal capture theories was minimal at low temperatures, while at higher temperatures short-range repulsive terms had more of an effect than did anisotropic potentials and are able to bring the calculated rate coefficients into agreement with experiment whereas the isotropic models yield a rate coefficient 3 times the measured one. Even at 300 K, the differences are not great. Here we used for simplicity an isotropic long-range $-Cr^{-6}$ attractive potential between a dipole and an induced dipole for the studied radiative association. With this potential, L_{max} is given by

$$L_{max}(L_{max} + 1) = 32C^{1/3}\mu\hbar^{-2}E_{coll}^{2/3} \quad (5)$$

with

$$C = \frac{3}{2}\frac{I_A I_B}{(I_A + I_B)}\alpha_A\alpha_B + \mu_B^2\alpha_B. \quad (6)$$

Here E_{coll} is the initial translational energy of the reactants, μ is the reduced mass of the reactants, α is the dipole polarizability of the reactant in question, μ_B is the dipole of polar neutral reactant B, and I_A and I_B are the ionization potentials.

The rate coefficient for complex redissociation into reactants $k_{-1}(J, E)$, where E is the total energy, can be obtained using microscopic reversibility and the energy density (see Light 1967; Klots 1971; Herbst 1985). The rather complex expression is given by the equation

$$k_{-1} = \frac{1}{h(2J + 1)\rho_v(E_{vib}/\sigma)}\sum_{J'_A}\sum_{J'_B}\sum_{vib} \times [(2J'_A + 1)(2J'_B + 1)/\sigma_A\sigma_B]\sum_{L'}\sum_{J'_r}1 \quad (7)$$

for two nonlinear reactants, where ρ_v is the complex vibrational density of states, σ_A and σ_B are the symmetry numbers for the reactants (here, the "products" of redissociation), and J'_A, J'_B, J'_r, and L' are the product quantum numbers analogous to those for complex formation. The product channel obeys a triangle rule with J'_A and J'_B adding vectorially to possible values of J'_r, and J'_r and L' adding vectorially to J. Any available vibrational states of A and B after redissociation of the complex are included in the summation over "vib." The complex density of vibrational states, ρ_v, is adapted from the rovibrational density used in the initial canonical equilibrium theory of radiative association (Herbst 1979). Deletion of the

rotational states as done by Marcus & Rice (1951) leads to:

$$\rho_\nu = \frac{(D_0 + V_{\rm eff} - E_{\rm rot} + E_z)^{s-1}}{s! hc\sigma \sum_i h\nu_i}, \quad (8)$$

where D_0 is the strength of the complex bond formed, $V_{\rm eff}$ is the effective maximum potential energy, combining the centrifugal barrier and the long-range potential, s is the number of vibrational degrees of freedom, σ is the complex symmetry number, and the ν_i are the frequencies of the vibrational modes of the complex.

Once a collision complex is formed, it can redissociate into reactants or emit a photon and thereby stabilize the complex and complete the process of radiative association. In some cases, there is a third option, as mentioned in the 1, and contained in the k_2 term of Equation (2) of dissociation of the complex to form at least one exothermic two-body product channel. The rate of formation of new products depends on the energy barrier in excess of the product energy via the RRKM treatment (Miller 1979):

$$k_2 = \frac{(s-1)! \prod_i^s \hbar\nu_i}{2\pi\hbar E^{s-1}} \sum_n P(E_{1,n}), \quad (9)$$

where s is the number of modes in the complex and therefore s-1 is the number of modes in the transition state, ν_i are the vibrational modes of the complex, $\nu_i^{\#}$ are the vibrational modes of the transition state, E is the energy of the complex, and $P(E_1, n)$ is the probability of tunneling through a particular mode dependent on the energy in that mode, E_1, as given in Miller (1979).

Another consideration for the collision complex is that it may "roam" into other channels on other reaction pathways. Because roaming is not a standard part of a phase-space theory, any information about roaming channels is best included with a roaming rate coefficient directly from the results of roaming calculations, and added to the k_2 term of Equation (1). This is discussed in more detail in Section 3.

Radiative association also depends on the rate of stabilizing emission. Stabilizing emission is most likely to come through an infrared-active channel, and larger molecules are more likely to have more of these. As shown by Herbst (1982), the rate coefficient of radiative stabilization $k_{\rm r}$ can be approximated by the harmonic formula

$$k_r = \frac{E_{\rm vib}}{s} \sum_{i=1}^{s} \frac{A_{1\rightarrow 0}^{(i)}}{h\nu_i}, \quad (10)$$

where $E_{\rm vib}$ is the vibrational energy of the complex, s is the number of vibrational modes in the collision complex, ν_i are the vibrational frequencies, and each $A^{(i)}$ is the Einstein A coefficient for emission from the first excited vibrational state of mode i to the ground vibrational state. The Einstein A coefficients are given by

$$A_{1\rightarrow 0}^{(i)} = \frac{8\pi}{c} \nu_i^2 I, \quad (11)$$

where I is the intensity in units of km mol^{-1} (Herbst 1982). This formula contains the assumption that the complex can be stabilized by the emission of a single photon; that is, that the complex lies above the dissociation limit of the stable molecule, but the emission of a single photon brings the complex below the dissociation energy.

While the harmonic approximation serves as a good estimate, the emission rate coefficient k_r can increase with anharmonic contributions. Since the overall radiative association rate coefficient $k_{\rm ra}$ scales with the emission rate as long as it does not become very large so as to dominate the denominator of Equation (1), the results given below can be considered conservative estimates of the radiative association rate coefficient and anharmonic terms can contribute as much as a factor of 5 to the overall rate coefficient. The multiple and sometimes competing effects of anharmonicity are discussed in Herbst (1982).

The microcanonical phase-space approach depends on the amount of energy contained in the system of nine atoms in a CH_3OCH_3 collision complex, but models of the ISM are more often described by one temperature. To achieve this change, each of the constituent rate coefficient terms in Equation (1) is calculated at a particular energy and angular momentum, with the incoming rotational energies from the reactant angular momenta J_A and J_B factored out and considered separately. $k_{\rm ra}$ is found for each combination of translational energy, angular momentum, J_A and J_B, and summed over each accessible value of J from 0 to $J_{\rm max}$. Then, each $k_{\rm ra}$ is integrated according to a Maxwell–Boltzmann distribution from 0 to 12 kT. These bounds allow for every value of the energy to be considered, though the higher energies are weighted more lightly since they are relatively unlikely. This gives a thermalized value of $k_{\rm ra}$, and rotational populations are the last consideration. The relative contributions for each possible value of angular momenta J_A and J_B are weighted by the probabilities of finding each reactant in the particular rotational state, so that higher rotational levels also contribute less to the total overall rate.

To get a sense of the uncertainty of our phase-space results, we have also performed calculations by adapting a simpler canonical theory in which the ratio of k_1 to k_{-1} is treated by canonical partition functions. Based on prior calculations on both radiative and three-body association on ion–neutral systems, the results of this canonical theory are likely to be upper limits (Herbst 1980).

3. Results

The parameters needed to carry out the calculations for the processes described above are given in Table 1, where cgs-esu units are given to calculate the potential. The various parameters of the species were calculated at the density functional theory (DFT) level with the hybrid M06-2X functional developed by Zhao & Truhlar (2008), which is well suited for calculations involving main-group thermochemistry, associated with the aug-cc-pVTZ basis set using Gaussian09 (Frisch et al. 2016).

Following the processes described in Section 2 above, the radiative association rate coefficient was calculated for the temperature range of 10–300 K. The radiative association rate coefficients as a function of temperature between the methyl and methoxy radicals, as calculated with the phase-space approach and with the older canonical approach (Herbst 1980) are listed in Table 2, and shown in Figure 1.

As expected, there is an overall negative temperature dependence, which is roughly the same for the canonical and phase-space rate coefficients (see Figure 1), though the canonical rate coefficient is larger by a factor of 6–10 in the

Table 1
Molecular Parameters Used in Calculations

Species	Parameter Value
	Ionization Potential (eV)[a]
CH_3	9.842
CH_3O	10.72
	Polarizability (cm^3)[a]
CH_3	2.335×10^{-24}
CH_3O	3.089×10^{-24}
	Dipole Moment (Debye)[a]
CH_3O	2.7065
	Electronic Degeneracy[a,b]
CH_3	2
CH_3O	2
CH_3OCH_3*	1
	Total Energy at 0 K (kcal mol^{-1})[c]
CH_3	24987.6108
CH_3O	72225.965573
CH_3OCH_3	97320.379768
	Well Depth (kcal mol^{-1})[a]
Collision Complex	83.19
	Rotational Constants (cm^{-1})[c,d]
CH_3	9.45, 4.725
CH_3O	5.198, 0.987
CH_3OCH_3	0.505
	Vibrational Modes (cm^{-1})[d]
CH_3	523.7581, 1415.5889, 1415.6093, 3133.4106, 3310.4496, 3310.7025
CH_3O	754.3471, 972.9141, 1137.2748, 1384.2731, 1389.6156, 1516.7122, 2963.9264, 3033.8271, 3077.0303
CH_3OCH_3	222.1194, 270.1842, 426.4228, 983.0668, 1137.976, 1174.0569, 1204.9337, 1237.4963, 1279.2369, 1463.05, 1496.1804, 1496.8319, 1503.3653, 1507.4301, 1519.459,3011.2543, 3019.164, 3061.9497, 3067.8806, 3142.9954, 3144.0552
$CH_3OCH_3^{\#}$	1647.9055i[d], 307.8435, 321.9863, 458.7175, 777.015, 942.1068, 1022.9967, 1152.4847, 1192.5049, 1270.5918, 1364.4524, 1403.0082, 1467.6793, 1481.8891, 1530.5725, 2265.3745, 2836.3531, 2950.971, 3061.285, 3216.8511, 3288.5714
	Radiative Intensity (kml mol^{-1})
CH_3OCH_3	0.0, 5.3022, 2.9165, 35.4504, 18.4772, 0.0, 7.8391, 128.1823, 8.2952, 2.0703, 0.0, 0.0688, 11.573, 14.9355, 4.0265, 48.0799, 50.0564, 97.8169, 0.0002, 22.3102, 15.1701

Notes.
[a] Johnson (2020).
[b] Ground electronic state assumed.
[c] Radicals are treated as symmetric tops; dimethyl ether is treated as a spherical top using the geometric mean (this work).
[d] This imaginary frequency is used only in the calculation of the tunneling rate under the transition state barrier leading from the complex to the competitive exit channel. The transition state is labeled with the # sign.

range 10–100 K. The radical–radical combination lends this reaction a particularly deep energy well, creating a long-lived

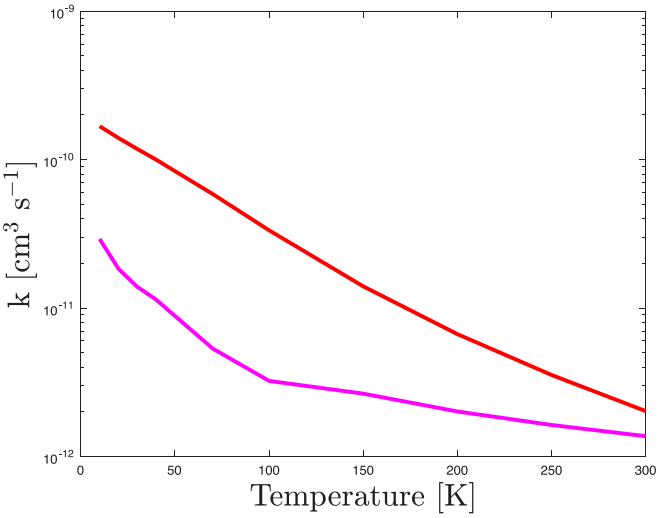

Figure 1. Canonical (red) and phase-space (magenta) results for the radiative association rate coefficient between methyl and methoxy radicals, from 10 to 300 K.

Table 2
Results for Methyl–Methoxy Radiative Association Rate Coefficients as a Function of Temperature

Temperature (K)	Canonical k_{ra} (cm^3 s^{-1})	Phase-space k_{ra} (cm^3 s^{-1})
10	1.68(−10)	2.92(−11)
20	1.40(−10)	1.84(−11)
30	1.18 (−10)	1.39(−11)
40	1.00(−10)	1.14(−11)
70	5.87(−11)	5.34(−12)
100	3.34(−11)	3.23(−12)
150	1.40(−11)	2.65(−12)
200	6.67(−12)	2.01(−12)
250	3.54(−12)	1.63(−12)
300	2.02(−12)	1.37(−12)

Note. a(b) indicates a $\times 10^b$.

complex, up to the order of 1 s at the lowest temperature investigated, capable of producing dimethyl ether. This reaction also benefits from a high energy barrier in the bimolecular exit channel, which reduces k_2 to irrelevance. The radiative association rate coefficients, especially the canonical result, even approach the collisional rate coefficient at 10 K.

The quantitative discussion up to now has ignored the phenomenon of roaming. A roaming channel does appear to exist for this reaction (Tsang & Hampson 1986; Sivaramakrishnan et al. 2011). The roaming pathway was tested at higher energies, equivalent to 251–755 K, so that the smaller temperatures considered here require some extrapolation. However, the roaming pathway appears to be entirely first order and increasing with temperature, and the rates for this process are quite small at low temperatures. The first-order rate coefficient (s^{-1}) is given by the equation

$$k_{2,\mathrm{roaming}} = 2955.79E^{0.780}, \quad (12)$$

where E is the energy per kcal mol^{-1}, which when multiplied by the pre-exponential constant gives s^{-1}.

Since roaming is a competitive pathway with radiative association, this rate coefficient is added into the denominator of Equation (1). The effect of this addition, which has already

Table 3
Modified Arrhenius Rate Expressions for Methyl–Methoxy Radiative Association[a]

α (cm^3 s^{-1})	β	γ	
1.37(−12)	−0.96	0.00	This work, phase-space
1.70(−11)	−0.70	0.00	This work, canonical
1.00(−15)	−3.00	0.00	Vasyunin & Herbst (2013)
1.00(−14)	−3.00	0.00	Balucani et al. (2015)

Note. These fits apply to the temperature range 10–100 K.
[a] a(b) indicates a × 10^b.

been included within the results shown in Table 2, is minimal, though nonzero, simply because the rate for k_{-1} also rises and rises much more quickly with energy. Thus, although roaming can happen effectively at higher energies, a collision complex is still more likely to redissociate than to roam. As with the other constituent rate coefficients in Equation (1), the roaming rate coefficients are calculated at a particular energy and then included in k_{ra}, which is then integrated to an equivalent temperature. Using this process, Equation (12) yields a roaming rate coefficient of 139 s^{-1} at 10 K, 488 s^{-1} at 50 K, 838 s^{-1} at 100 K, and 1980 s^{-1} at 300 K. At the same time, k_{-1} is on the order of 100 s^{-1} at 10 K, but 10^6 s^{-1} at 100 K, though the precise value is dependent on the J and E values being considered, as discussed above. The roaming channel has been included for every result in Table 2; it exceeds the more direct approach to products CH_4 and CH_2O.

To determine whether or not methyl–methoxy radical radiative association could enhance the calculated abundance of dimethyl ether sufficiently to explain its abundance in a number of sources, the newly calculated rate coefficients and previously reported estimates (Balucani et al. 2015; Vasyunin & Herbst 2013) were fitted to a modified Arrhenius equation:

$$k_{ra} = \alpha\left(\frac{T}{300\ \mathrm{K}}\right)^{\beta} \exp(-\gamma/T) \tag{13}$$

so that they could be included in the NAUTILUS-1.1 chemical model (Ruaud et al. 2016). The fitted values are listed in Table 3, and represent the calculated rate coefficients from 10 to 100 K.

Previous work by Balucani et al. (2015) using an augmented version of the OSU2009 network indicates that raising the radiative association rate coefficient from the Vasyunin & Herbst (2013) estimate of 3×10^{-11} cm^3 s^{-1} at 10 K by an order of magnitude increases the net production of dimethyl ether such that the radiative association can explain the abundance of dimethyl ether in L1544, a rather complex source. The rate coefficient used by Balucani et al. (2015) is very close to our canonical value at 10 K. Nevertheless, with the use of the NAUTILUS network at this temperature, we find that inclusion of either our canonical or phase-space rate coefficient does not appreciably change the predicted abundance of dimethyl ether, showing that other mechanisms are more important.

4. Discussion and Conclusions

The result of both a phase space and a canonical calculation of the radiative association rate coefficient between the neutral methyl and methoxy radicals to form dimethyl ether shows that the reaction rate coefficient for these radicals can be quite high at low temperatures, as compared with other radiative association reactions in the NAUTILUS network (Ruaud et al. 2016). Though methyl has not yet been observed in cold regions, its abundance has been predicted (McGuire et al. 2017). The methoxy radical has been seen toward the dark cloud B1-b at a derived fractional abundance with respect to total hydrogen of 4.67×10^{-12} (Cernicharo et al. 2010). The fractional abundances of these radicals in the Nautilus model, for standard cold core conditions, lie in the 10^{-8} to 10^{-10} range at the relevant timescale for observation of dimethyl ether. Nevertheless, using the calculated abundances of the methyl and methoxy radicals even with the largest of the above reaction rate coefficients at 10 K we were not able to account fully for the observed abundance of dimethyl ether solely with formation by radiative association. The production of dimethyl ether by radiative association using Nautilus appears to be too slow at 10 K to explain fully the abundance of dimethyl ether, especially in cold sources with higher abundances such as TMC-1, unless other mechanisms can add to its synthetic power.

As shown in Figure 2, there is only a small difference in the peak-time abundances of dimethyl ether when we compare plots using the NAUTILUS network with the radiative association completely turned off (RAoff), with the phase-space (PS) value used, and with the larger canonical value used. In the TMC-1 models considered here, the radiative association reaction accounts for approximately 1% of the total dimethyl ether produced at peak time. Specifically, at the peak time, use of the canonical rate leads to a peak-time fractional abundance of 2.104×10^{-10} while use of the phase-space rate leads to a peak-time fractional abundance of 2.093×10^{-10}. These can be compared with a peak-time fractional abundance without the radiative association of 2.090×10^{-10}. At 10 K, the phase-space calculation of the rate is about an order of magnitude slower than the canonical theory, but the difference in peak gas-phase fractional abundance of dimethyl ether between the theories considered in the paper is on the order of 10^{-12}, though the peak abundance is on the order 10^{-10} with or without the radiative association. Observational estimates of the fractional abundance of dimethyl ether in TMC-1, a standard cold core, range from 1.5×10^{-10} (Soma et al. 2018) to 2.5×10^{-10} (Agúndez et al. 2021) on the cyanopolyyne peak, meaning that the models considered here all fall within the range of the observations, although this agreement has little to do with the radiative association rate coefficients. Instead, the two reactions that can account for the observed abundance of dimethyl ether are the reactive (chemical) desorption processes

$$CH_3(s) + CH_3O\ (s) \rightarrow CH_3OCH_3\ (g), \tag{14}$$

and

$$H\ (s) + CH_3OCH_2(s) \rightarrow CH_3OCH_3\ (g), \tag{15}$$

in which radicals on a grain surface combine and the exothermicity of the reactions subsequently allows desorption of the products from the grain into the gas phase at an assumed value of 1%.

Recently, Jin & Garrod (2020) have introduced an interesting potential mechanism, whereby a hydrogen atom reacts with a CH_2 radical on a grain surface, and the new CH_3 radical reacts instantaneously with a nearby CH_3O radical to form dimethyl ether, possibly significantly increasing the gas-phase

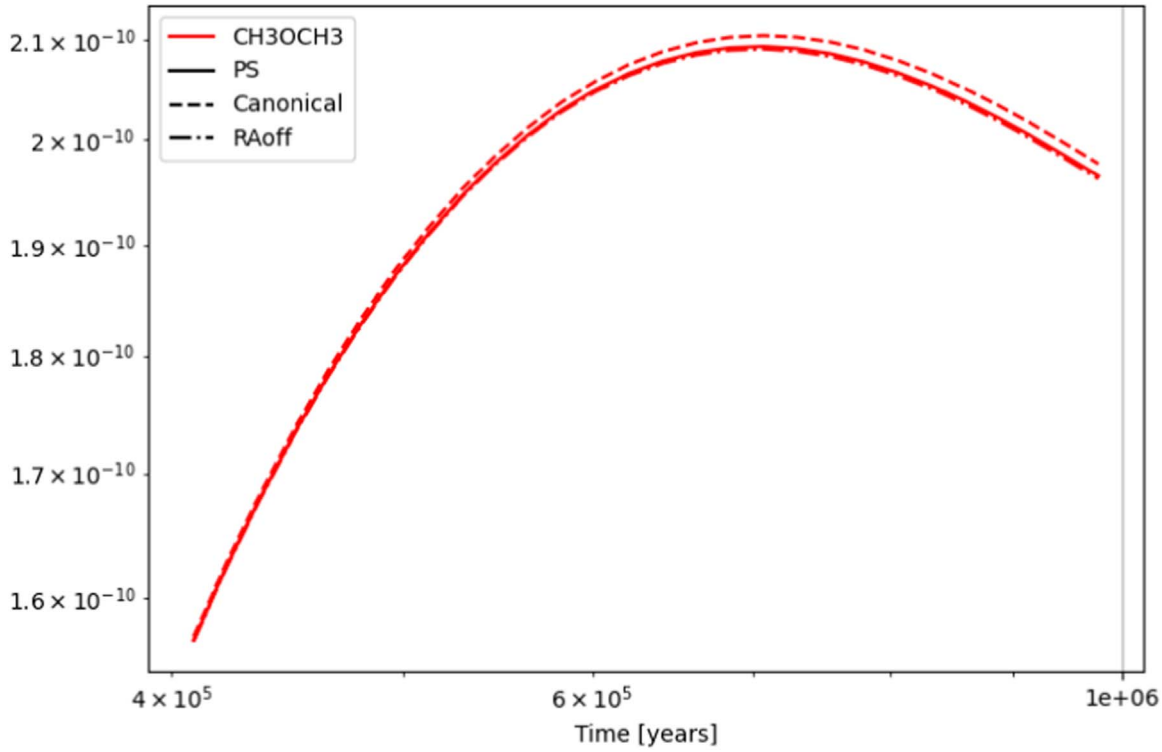

Figure 2. Gas-phase fractional abundances with respect to total hydrogen for dimethyl ether as a function of time using the Nautilus network under cold core conditions. Results are shown with the phase-space and canonical (thermal) theories developed for the rate of radiative association and for a model without the radiative association of dimethyl ether (RAoff). As noted above, the peak abundances here are in line with the observed abundance of dimethyl ether in TMC-1 and other prestellar cores.

abundance of dimethyl ether by chemical desorption. Similar other processess involving three bodies can play a role in the formation of other COMs. Radiative association may still play a role in the formation of COMs, especially since the catalog of such gas-phase reactions obtained by calculations between neutral radicals is currently incomplete. An alternative route for the production of CH_3OCH_3 could be the radiative association between $CH_3^+ + CH_3OH$ giving $CH_3OHCH_3^+$ followed by the dissociative electron recombination of $CH_3OHCH_3^+$, although this dissociative recombination yields only the low fraction of 7% dimethyl ether (Hamberg et al. 2010). The reaction to form $CH_3OHCH_3^+$ competes with the transfer of H^- giving $H_2COH^+ + CH_4$ (Herbst 1987). The calculated rate for the formation of $CH_3OHCH_3^+$ is not sufficient to explain the formation of CH_3OCH_3 but great uncertainties exist on the precise value of this rate. Another interesting factor to consider is the recent work on radiolysis (Paulive et al. 2021). Radiolysis, the collective term for nonthermal processes by which molecules on and in grain mantles are ionized and excited by cosmic rays, can result in a temporary increase in the abundance of radicals on surfaces or in the gas-phase. This, then, can drive up production of COMs through other reaction pathways. As an understanding of the assorted mechanisms to form COMs under both cold and warm environments continues to grow, an increase in the the list of studied radiative association reactions between neutral species will prove valuable.

We would like to thank S. J. Klippenstein for valuable conversations on the topic of roaming, especially within this reaction pathway. E.H. thanks the National Science Foundation for support of his program in astrochemistry via grant AST 19-06489.

ORCID iDs

Jessica Tennis https://orcid.org/0000-0003-2245-4233
Jean-Christophe Loison https://orcid.org/0000-0001-8063-8685
Eric Herbst https://orcid.org/0000-0002-4649-2536

References

Agúndez, M., Marcelino, N., Cernicharo, J., Roueff, E., & Tafalla, M. 2019, A&A, 625, A147
Agúndez, M., Marcelino, N., Tercero, B., et al. 2021, A&A, 649, L4
Bacmann, A., Taquet, V., Faure, A., Kahane, C., & Ceccarelli, C. 2012, A&A, 541, 1
Balucani, N., Ceccarelli, C., & Taquet, V. 2015, MNRAS, 449, 16
Cernicharo, J., Marcelino, N., Roueff, E., et al. 2010, ApJL, 759, L1
Feuchtgruber, H., Helmich, F. P., van Dishoeck, E. F., & Wright, C. M. 2000, ApJL, 535, L111
Frisch, M. J., Trucks, G. W., Schlegel, H. B., et al. 2016, Gaussian09 Revision A.02 (Wallingford, CA: Gaussian Inc.)
Garrod, R. T., Widicus-Weaver, S. L., & Herbst, E. 2008, ApJ, 682, 283
Hamberg, M., Österdahl, F., Thomas, R. D., et al. 2010, A&A, 514, A83
Herbst, E. 1979, JChPh, 70, 2201
Herbst, E. 1980, ApJ, 237, 462
Herbst, E. 1982, JChPh, 65, 185
Herbst, E. 1985, A&A, 153, 151
Herbst, E. 1987, ApJ, 313, 867
Jaber, A. A., Ceccarelli, C., Kahane, C., & Caux, E. 2014, ApJ, 791, 1
Jin, M., & Garrod, R. T. 2020, ApJS, 249, 26
Johnson, R. D., III 2020, NIST Computational Chemistry Comparison and Benchmark Database NIST Standard Reference Database Number 101, http://cccbdb.nist.gov/
Klots, C. E. 1971, JPCA, 75, 1526
Liao, Q., & Herbst, E. 1995, ApJ, 444, 694
Light, J. C. 1967, Disc. Faraday Society, 44, 14
Marcus, R. A., & Rice, O. K. 1951, JPCA, 55, 894
McGuire, B. A., Shingledecker, C. N., Willis, E. R., et al. 2017, ApJL, 851, L1
Miller, W. H. 1979, JACS, 101, 6810

Öberg, K. I., Bottinelli, S., Jørgensen, J. K., & van Dishoeck, E. F. 2010, ApJ, 716, 825
Paulive, A., Shingledecker, C. N., & Herbst, E. 2021, MNRAS, 500, 3414
Ruaud, M., Wakelam, V., & Hersant, F. 2016, MNRAS, 459, 3756
Sivaramakrishnan, R., Michael, J. V., Wagner, A. F., et al. 2011, CoFl, 158, 618
Soma, T., Sakai, N., Watanabe, Y., & Yamamoto1, S. 2018, ApJ, 854, 116
Taquet, V., Wirström, E. S., Charnley, S. B., et al. 2017, A&A, 607, A20
Tsang, W., & Hampson, R. F. 1986, JPCRD, 15, 1087
Vastel, C., Ceccarelli, C., Lefloch, B., & Bachiller, R. 2014, ApJL, 795, L1
Vasyunin, A. I., & Herbst, E. 2013, ApJ, 769, 34
Zhao, Y., & Truhlar, D. G. 2008, Theoretical Chemistry Accounts, 120, 215